

MAHRSI observations of nitric oxide in the mesosphere and lower thermosphere

Michael H. Stevens, Robert R. Conway

E. O. Hulburt Center for Space Research, Naval Research Laboratory

Joel G. Cardon

Computational Physics, Inc.

James M. Russell III

Department of Physics, Hampton University

Abstract. In November, 1994, the Middle Atmosphere High Resolution Spectrograph Investigation (MAHRSI) observed the distribution of NO between the altitudes of 76 and 140 km by measuring limb intensity profiles of solar resonance fluorescence in the NO $A^2\Sigma \rightarrow X^2\Pi$ (1,0) γ band near 215 nm. The observations were made from the ASTRO-SPAS (Shuttle Pallet Satellite) spacecraft which was deployed and retrieved by the space shuttle. The data provided a seven hour snapshot of lower thermospheric and mesospheric NO from sunrise near 48° S to sunset near 61° N latitude following a period of low solar and high geomagnetic activity. Inferred peak lower thermospheric NO densities ranged from 3×10^7 cm⁻³ near the equator to 2×10^8 cm⁻³ at high northern latitudes, roughly consistent with previous observations for the same conditions. Individual vertical density profiles showed substantial structure and large orbit to orbit variations, suggesting that the distribution of mesospheric and lower thermospheric NO is dynamically influenced.

Introduction

Since the first observation of NO in the atmosphere by Barth [1964], results from several experiments using a variety of techniques have demonstrated that its distribution in the thermosphere and mesosphere is highly variable. Rusch [1973] showed that the lower thermospheric distribution at high latitudes has a strong dependence on geomagnetic activity while Barth *et al.* [1988] observed that NO at equatorial latitudes shows a clear response to solar activity. Cravens and Stewart [1978] showed that the global distribution of NO in the lower thermosphere is asymmetric about the geographic and geomagnetic poles and suggested that horizontal transport was responsible. The Halogen Occultation Experiment (HALOE) on NASA's Upper Atmosphere Research Satellite (UARS) has acquired an extensive record of the global variability of NO throughout the middle atmosphere and lower thermosphere during its six years of operations [Russell *et al.*, 1993]. Because HALOE uses the solar occultation technique, however, it requires many weeks to provide extensive global cov-

erage. The study of NO suffers from the lack of nearly synoptic observations with high spatial resolution to help quantify all of the processes that determine its global distribution [Cravens *et al.*, 1985].

We report here MAHRSI observations of NO $A^2\Sigma \rightarrow X^2\Pi$ (1,0) γ band solar fluorescence near 215 nm for five sequential orbits on November 6-7, 1994. During these observations, the local time varied from sunrise at high southern latitudes to sunset at high northern latitudes. The solar activity was low (F10.7 = 91) whereas the K_p index had peaked at 6 twelve hours earlier, indicating that geomagnetic activity was relatively high. The high spatial resolution of the data reveals large orbit to orbit variations of NO at most latitudes and altitudes.

The Experiment

MAHRSI is an ultraviolet spectrograph experiment with a spectral resolution of about 0.03 nm near 215 nm. The instrument uses an intensified CCD detector and is sensitive between 190 and 320 nm. MAHRSI conducted a joint mission with the Cryogenic Infrared Spectrometers and Telescopes for the Atmosphere (CRISTA) experiment and was deployed into a 300 km orbit with an inclination of 57°. Mesospheric OH observations during this flight are reported by Conway *et al.* [1996]. Altitude scans of NO γ (1,0) solar fluorescence between 76 and 140 km were obtained every 88 sec by scanning the $1.15 \times 0.01^\circ$ field of view in 2 km steps. The field of view projected to a tangent height of 100 km subtends less than 0.3 km in the vertical. Post-flight spacecraft attitude data show that the uncertainty of the observed tangent height was about 0.25 km. MAHRSI observed the γ (1,0) band at a rate of about one scan every 4° in latitude between 48° S and 61° N for about 30 sunlit scans per orbit. Individual orbital ground tracks are parallel, about 23° apart in longitude, and about 1.5 hours apart in elapsed time.

The pre and post-flight calibration of the instrument, including the rejection of off-axis light are described in Conway *et al.* [1996]. The relative response of the instrument to a D₂ source was normalized between 280 and 320 nm to the absolute response measured using a calibrated quartz halogen radiance source. The resulting estimate of the responsivity at 215 nm was 73.8 dn/pixel/sec/(kR/0.01 nm), where 1 photo-event produces 13.1 dn. The postflight calibration showed that the responsivity at 215 nm was lower by 12%. We estimate that the accuracy of the calibration is (+3, -14)%.

Copyright 1997 by the American Geophysical Union.

Paper number 97GL03257.
0094-8534/97/97GL-03257\$05.00

Data Analysis

Both the $\gamma(1,0)$ rotational emission rate factors (g-factors) and self-absorption cross sections required for the interpretation of the observed intensities were calculated using the procedure of Stevens [1995]. For the g-factor calculation, the solar irradiance measurement of Hall and Anderson [1991] was normalized to the exoatmospheric measurement of the Solar Stellar Intercomparison Experiment (SOLSTICE) coincident in time to the MAHRSI observations [Rottman et al., 1993; Woods et al., 1996]. The $\gamma(1,0)$ band g-factor was 6.77×10^{-6} photons/s at 200 K.

Both g-factors and self-absorption cross sections were calculated in 10–20° K increments and interpolated onto MSIS model temperatures at each altitude [Hedin, 1991]. To infer $\gamma(1,0)$ radiances from the limb observations, rotational emission spectra were calculated, convolved with laboratory measured spectral resolution functions, and scaled to fit the data in a least-squares sense. Since both temperature and self-absorption affect the shape of the emission band, a different rotational spectrum was calculated with representative NO densities for each altitude in 10° latitude bins from 50° S to 60° N. A MAHRSI $\gamma(1,0)$ spectrum is shown in Figure 1 along with two model spectra, one optically thin and one with self-absorption.

A least-squares fitting algorithm was used to separate the $\gamma(1,0)$ radiances from other contributions in the passband, including the NII doublet near 214 nm and Rayleigh scattered sunlight. The NII doublet at 213.97 nm and 214.35 nm is resolved at the highest altitudes observed and each line was modeled using the MAHRSI spectral resolution function. The two features were then independently fit to the data and removed before calculating the γ band intensity. The total intensity of the doublet is less than 2 kR at all altitudes,

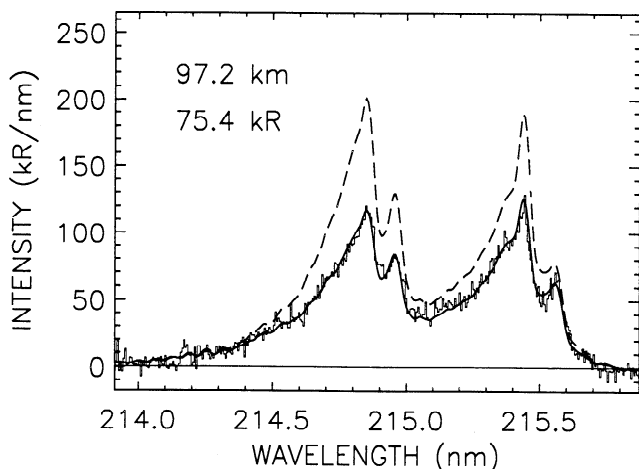


Figure 1. A MAHRSI $\gamma(1,0)$ band spectrum (histogram) from fourteen scans averaged between 45° N and 55° N latitude. The theoretical prediction of the $\gamma(1,0)$ spectrum convolved with the MAHRSI spectral resolution function is the smooth solid curve and the optically thin result (without self-absorption) is the smoothed dashed curve. The observed spectrum is calculated to be 31% self-absorbed. Note that the relative intensity of the sub-bands changes with increased self-absorption.

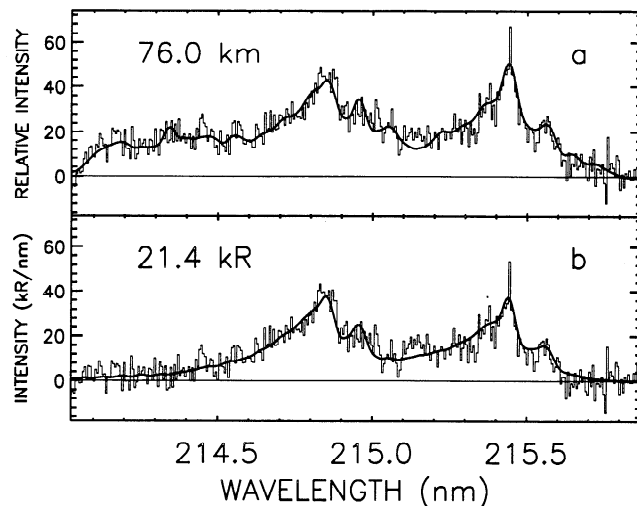


Figure 2. a. A MAHRSI spectrum at 76 km and the least squares fit to the data including both Rayleigh scattered sunlight and the $\gamma(1,0)$ band. The data are an average of MAHRSI spectra near 30° N. b. Figure 2a with the modeled Rayleigh scattered sunlight subtracted.

consistent with previous observations for low solar activity [Torr and Torr, 1985], but small compared to the $\gamma(1,0)$ band intensities at most altitudes observed. The spectrum of Rayleigh scattered sunlight is present in the data at tangent heights below 100 km. The high spectral resolution of MAHRSI helped to remove this highly structured spectrum from the observation with precision, thereby allowing for retrievals of NO down to 76 km. The Rayleigh scattering contribution was estimated by convolving the irradiance measurement of Hall and Anderson [1991] with the MAHRSI spectral resolution functions and fitting the resulting shape to the data between 76–100 km. A MAHRSI spectrum is shown in Figures 2a and 2b with and without Rayleigh scattering, illustrating that the shape of the $\gamma(1,0)$ band may be reliably distinguished from the shape of the Rayleigh scattered background using the least-squares technique. A baseline continuum was included in the spectral fitting algorithm in part to account for small uncertainties in dark field obtained on orbit. This continuum typically had a value of less than 1% of the subtracted dark field.

NO density profiles were obtained by inverting individual altitude profiles of the γ band radiances using a Twomey regularization scheme [Twomey, 1977] which was constrained by the smoothness of the profile and included self-absorption. The weighting functions are strongly peaked at the minimum tangent ray height and their full-width at half-maximum is about 6 km. The inversion incrementally includes all contributions to the NO emission and self-absorption both across the band at milliÅngstrom intervals and along the line of sight. The resulting high resolution spectra were integrated over wavelength to obtain model band intensities which were compared to the data.

The peak signal-to-noise ratio from any single profile ranges from about 20 at low latitudes and low NO densities to about 70 at high latitudes and high densities. The random measurement uncertainty consists primarily of detector noise and photon shot noise. The

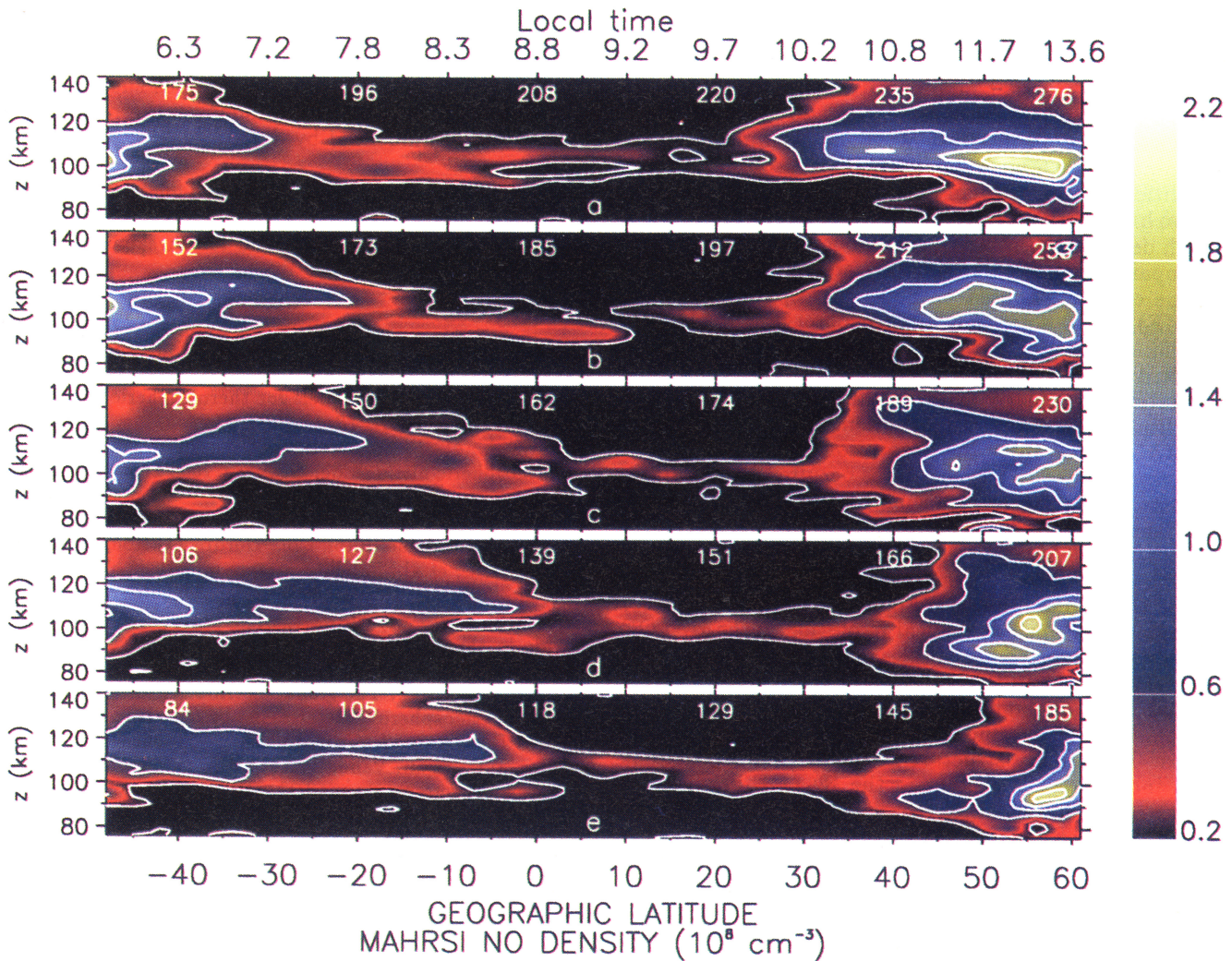


Figure 3. NO densities inferred from MAHRSI Orbits 50 (3a) through 54 (3e). The geographic longitudes are included at the top of each panel (in °E). Random uncertainties are in general less than $5 \times 10^6 \text{ cm}^{-3}$.

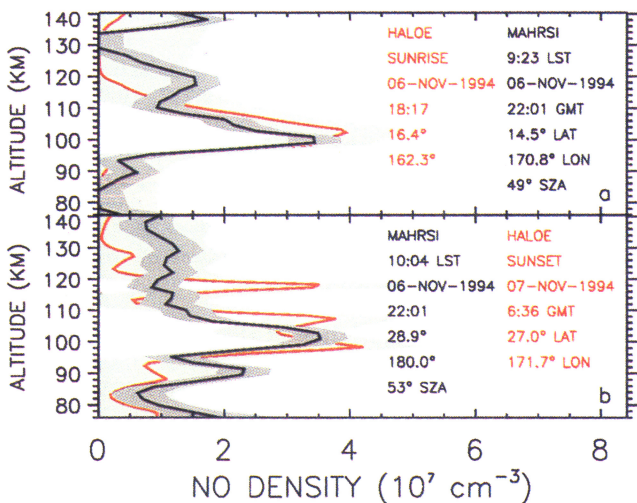


Figure 4. MAHRSI/HALOE comparison where the geographic location of the 109 km tangent height for each scan is shown. Both Figures 4a and 4b compare profiles that are less than 1000 km apart. Both MAHRSI profiles are from Orbit 52 (Figure 3c). 1 σ random uncertainties are shaded for each profile.

uncertainty is at most 23% but is typically a few percent and is propagated through the inversion to estimate the random uncertainty at each tangent height. Systematic uncertainties include the calibration, laboratory measurements of the oscillator strength (5%) and branching ratio (5%) required for the g-factor calculations, and the SOLSTICE absolute solar irradiance (2%). The total systematic uncertainty is therefore estimated to be (+15%, -26%).

Results

Figures 3a-3e show NO number densities inferred as a function of latitude and altitude for each orbit in chronological order from top (MAHRSI Orbit 50) to bottom (Orbit 54). Note that the progression of local time with latitude is indicated on the top axis and is the same for each orbit. In general, Figure 3 shows the well known increase in lower thermospheric densities from low to high latitudes, with a peak of $3 \times 10^7 \text{ cm}^{-3}$ near the equator and $2 \times 10^8 \text{ cm}^{-3}$ at high northern latitudes. Both peak values are roughly consistent with previous observations for low solar and high geomagnetic activity [Barth, 1996; Russell et al., 1993]. Also note in Figure 3 that higher densities are inferred in the

winter (northern) mesosphere than the summer mesosphere, as expected due to reduced photodissociation of NO during winter.

Figure 3, however, shows a remarkable amount of structure both vertically and meridionally. One prominent example is that high densities ($\geq 6 \times 10^7 \text{ cm}^{-3}$) in the southern hemisphere extend 25° further north in Orbit 54 than in Orbit 50. This asymmetry is not eliminated when viewed in geomagnetic coordinates. In addition, the $1 \times 10^8 \text{ cm}^{-3}$ contour in Orbit 50 extends from high northern latitudes down to about 33° N. Such high densities at mid-latitudes are a factor of 2-4 larger compared to Orbit 54 and to reference models for the same conditions based on Solar Mesospheric Explorer (SME) $\gamma(1,0)$ solar fluorescence observations [Barth, 1996]. Note also that the shape of the lower thermospheric peak in Figure 3 is subject to change from orbit to orbit, particularly at the highest latitudes, and that multiple peaks are not uncommon.

HALOE measures the absorption of sunlight by the $5.3 \mu\text{m}$ band of NO as the sun is occulted by the atmosphere during sunrise and sunset. Results from that experiment provide vertical mixing ratio profiles between about 10-150 km [Russell et al., 1993; Gordley et al., 1996]. Representative results from HALOE (Version 18) and MAHRSI are shown in Figures 4a (HALOE sunrise) and 4b (sunset). The vertical resolution of the HALOE and MAHRSI retrieved profiles is nearly the same. Note that MAHRSI and HALOE results are in general agreement and show highly structured vertical profiles with variations well beyond the random uncertainty of the data. The vertical structure in the MAHRSI profiles is not inconsistent with that in the HALOE profiles but since a smoothing constraint is imposed on all inversions, detailed comparison of the profiles at each altitude may be misleading. Systematic differences of a factor of two or more such as near 118 km in Figure 4b, however, cannot be reconciled regardless of the degree of smoothing employed. This suggests that the differences between the two observations are due to real variations in the distribution of NO.

Summary

The MAHRSI results presented here provide a seven hour snapshot of NO densities from high southern latitudes to high northern latitudes in the upper mesosphere and lower thermosphere. The observations followed a period of intense geomagnetic activity which was undoubtedly responsible for the high densities observed at auroral latitudes. Figure 3 summarizes the results and illustrates that the observations require analysis on an orbit to orbit basis to properly interpret the global distribution of NO. Because the typical chemical lifetime of NO is at least a day at these altitudes [Brasseur and Solomon, 1986], the orbit to orbit variation shown in Figure 3 cannot be completely produced by chemistry. However, care must be taken when interpreting the results because temporal and spatial variations are not distinguishable. The observed variations could be due to direct transport of NO during the 1.5 hours between orbits, a change in the background atmosphere to which NO is responding, static longitudinal asymmetry of the NO densities, or a combination of these possibilities. More comprehensive and synoptic NO observations will help to determine the relative contribution of the competing effects.

In general, peak lower thermospheric densities inferred from new MAHRSI NO observations of $\gamma(1,0)$

solar fluorescence show agreement with results from previous work under similar geophysical conditions both at high latitudes and near the equator. However, vertical structure present in the individual profiles, large orbit to orbit variations at most latitudes, and comparisons with coincident HALOE NO observations suggest that the distribution of mesospheric and lower thermospheric NO is strongly influenced by dynamics.

Acknowledgments. Several helpful discussions with D.E. Siskind and L.L. Gordley are gratefully acknowledged. We are also grateful to S.E. Zasadil for developing the inversion algorithm used in this work.

References

- Barth, C.A., Rocket measurements of the nitric oxide dayglow, *J. Geophys. Res.*, *69*, 3301-3303, 1964.
- Barth, C.A., Reference models for thermospheric nitric oxide, *Adv. Space Res.*, *18*, 179-208, 1996.
- Barth, C.A., et al., Solar-terrestrial coupling: low-latitude thermospheric nitric oxide, *Geophys. Res. Lett.*, *15*, 92-94, 1988.
- Brasseur, G., and S. Solomon, *Aeronomy of the Middle Atmosphere*, D. Reidel Publ. Co., Dordrecht, Holland, 1986.
- Conway, R.R., et al., Satellite measurements of hydroxyl in the mesosphere, *Geophys. Res. Lett.*, *23*, 2093-2096, 1996.
- Cravens, T.E. and A.I. Stewart, Global morphology of nitric oxide in the lower E region, *J. Geophys. Res.*, *83*, 2446-2452, 1978.
- Cravens, T.E., et al., The global distribution of nitric oxide in the thermosphere as determined by the atmospheric explorer D satellite, *J. Geophys. Res.*, *90*, 9862-9870, 1985.
- Gordley, L.L., et al., Validation of nitric oxide and nitrogen dioxide measurements made by the Halogen Occultation Experiment for UARS platform, *J. Geophys. Res.*, *101*, 10,241-10,266, 1996.
- Hall, L.A., and G.P. Anderson, High-resolution solar spectrum between 2000 and 3100 Å, *J. Geophys. Res.*, *96*, 12927-12931, 1991.
- Hedin, A.E., Extension of the MSIS thermosphere model into the middle and lower atmosphere, *J. Geophys. Res.*, *96*, 1159-1172, 1991.
- Rottman, G.J., et al., Solar-stellar irradiance comparison experiment 1, 1, Instrument design and operation, *J. Geophys. Res.*, *98*, 10667-10677, 1993.
- Rusch, D.W., Satellite ultraviolet measurements of nitric oxide fluorescence with a diffusive transport model, *J. Geophys. Res.*, *78*, 5676-5686, 1973.
- Russell, J.M. III, et al., The Halogen Occultation Experiment, *J. Geophys. Res.*, *98*, 10,777-10,797, 1993.
- Stevens, M.H., Nitric oxide γ band fluorescent scattering and self-absorption in the mesosphere and lower thermosphere, *J. Geophys. Res.*, *100*, 14735-14742, 1995.
- Torr, M.R., and D.G. Torr, The NII 2143-Å dayglow from Spacelab 1, *J. Geophys. Res.*, *90*, 6679-6683, 1985.
- Twomey, S., *Introduction to mathematics of inversion in remote sensing and indirect measurements*, Oxford, Elsevier, 1977.
- Woods, T.N., et al., Validation of the UARS solar ultraviolet irradiances: Comparison with the ATLAS 1 and 2 measurements, *J. Geophys. Res.*, *101*, 9541-9569, 1996.

R. R. Conway and M. H. Stevens, Code 7641, E. O. Hulburt Center for Space Research, Naval Research Laboratory, Washington, D.C. 20375 (e-mail: stevens@uap.nrl.navy.mil)

J. G. Cardon, Computational Physics, Inc., Fairfax, 23031
J. M. Russell III, Department of Physics, Hampton University, Hampton, VA 23668

(Received August 19, 1997; revised October 27, 1997; accepted October 30, 1997.)